Alzheimer's Research & Therapy

RESEARCH

Open Access

Exploring cellular heterogeneity: single-cell and spatial transcriptomics of Alzheimer's disease brains and iPSC-derived microglia

Anjali Garg[1,2], Sheeny Vo[3†], Iara D. De Souza[4†], Ayslan Castro Brant[4], Logan Brase[1,2], Ekaterina Aladyeva[1,2,4], Ricardo D.'O. Albanus[1,2], Aasritha Nallapu[1,2], Hongjun Fu[3,5] and Oscar Harari[1,2,4*]

Abstract

Background Microglia, the brain's resident immune cells, play a pivotal role in Alzheimer's disease (AD) pathogenesis. These cells exhibit diverse transcriptional states in response to neuroinflammatory stimuli, and characterizing these states is essential for understanding AD mechanisms.

Methods We integrated single-cell and spatial transcriptomic datasets from multiple cohorts and brain regions, encompassing both experimental models and human tissues. Findings were validated through immunostaining of human brain samples.

Results Our comprehensive atlas revealed pronounced heterogeneity among microglial states, with disease-associated microglia (DAM) significantly enriched in AD brains compared to controls. Spatial transcriptomics and immunohistochemistry demonstrated that DAM predominantly localize to external cortical layers and near amyloid plaques, whereas homeostatic microglia are more abundant in internal cortical layers and distal regions. Immunofluorescence staining for P2RY12 and CD68 confirmed these spatial distributions.

Conclusion By harmonizing single-cell and spatial transcriptomics, we provide a detailed atlas of microglial diversity, highlighting regional and pathological specificity of microglial states in AD.

Significance This work advances prior studies by mapping microglial transcriptional states across multiple human cohorts and experimental contexts, integrating spatial data to reveal novel anatomical patterns. The enrichment of DAM in external cortical layers and homeostatic microglia in internal layers represents a previously unreported finding with potential therapeutic implications. While not exhaustive of all microglial datasets, this study establishes the first integrated reference combining single-nucleus and spatial transcriptomics, underscoring the importance of linking microglial diversity to AD neuropathology and brain architecture.

Keywords Alzheimer's disease, Spatially resolved transcriptomics, Single-nucleus RNA-seq, Integration, Amyloid beta, Tau, Microglia, Immunofluorescence staining

†Sheeny Vo and Iara D. De Souza contributed equally to this work.

*Correspondence:
Oscar Harari
oscar.harari@osumc.edu

Full list of author information is available at the end of the article

Background

Alzheimer's disease (AD) is a complex and devastating neurodegenerative condition affecting millions globally. It is characterized by the accumulation of amyloid beta (Aβ) plaques, neurofibrillary tangles (NTFs), gliosis, and neuronal death, leading to cognitive impairment and dementia [1]. Microglia play a significant role in AD, contributing to inflammation, phagocytosis, and neurodegeneration [2]. These are the brain's resident immune cells and exhibit diverse morphology, physiology, and gene expression patterns, which are associated with specific phenotype [3–5]. Induced pluripotent stem cell-derived microglia-like cells (iPSC-derived MLC) have been shown to have a significant potential in modeling microglial behavior in vitro, offering new avenues for studying AD pathogenesis [6–8]. Moreover, high-throughput sequencing technologies, particularly single-cell RNA-sequencing (scRNA-seq) and spatially resolved transcriptomics (SRT) enable high-resolution mapping of cellular states and spatial distributions within human tissues, providing unprecedented insights into AD pathogenesis. Identifying and characterizing microglia transcriptional states holds great promise for understanding the underlying mechanisms of this neurodegenerative disease [9, 10]. Although substantial efforts have been devoted to investigating the transcriptional repertoire of microglia, in both postmortem brains and experimental models of Alzheimer's disease, the spatial distribution of microglia across different cortical regions still remains under-investigated.

While the pathological hallmarks of AD, such as Aβ plaques and misfolded tau proteins, are well-documented, several fundamental questions remain unanswered. These include which microglial transcriptional states are associated with early and late-onset Alzheimer's, how these states are distributed in the human brain, and how they relate to Aβ plaques and NTFs. Additionally, understanding the predominant transcriptional states across different cortical layers that correlate with high Aβ plaque and tangle burden could provide critical insights into disease progression. Similarly, it is critical to understand how experimental models in vitro recapitulate transcriptional states observed in ex vivo tissues. To address these questions, we study microglial transcriptional states across human and experimental model samples in AD.

Multiple studies have examined the heterogeneity of the human brain [11–13], but a systematic effort to integrate postmortem microglia data with experimental models, such as iPSC-derived microglia in culture or xenografted into mouse brains, is lacking. Given the inherent plasticity of microglia, it is crucial to assess how experimentally generated and manipulated microglia compare to those found in the human brain, and to identify specific brain regions associated with amyloid-beta pathology. We integrated microglial single-cell datasets from human and experimental models to capture novel insights of the heterogeneity of pathways, biological processes, and microglia transcriptional states present in AD pathology. This approach allowed identification of different transcriptional states associated with various stages of AD, such as Sporadic AD (sAD), presymptomatic, early, and late-stages of AD, and carriers of genetic mutation in *APP* and presenilins (autosomal dominant AD; ADAD), shedding light on the diversity of immune responses and molecular signatures in the context of the AD. Moreover, the integration of spatially resolved transcriptomics (SRT) from human Middle Temporal Gyrus (MTG) and frontal cortex (FC) provides a new means of understanding microglia in relation to the pathological features of the disease but also its distribution across the cortical layers. To validate transcriptomic predictions, we performed immunohistochemistry experiments to determine homeostatic microglia, Disease-associated microglia (DAM) and Aβ plaque distributions in human AD brains.

In summary, our findings emphasize the power of leveraging large and diverse single-cell and SRT datasets to advance our understanding of the molecular mechanisms underlying AD. These insights have implications for the development of targeted therapeutic approaches aimed at modulating neuroinflammatory processes and potentially altering the course of the disease. By serving as an atlas to translate findings from experimental models to postmortem human brain studies and vice versa, this research bridges the gap between basic science and clinical application, paving the way for developing new therapeutic strategies in AD.

Methods

Single cell datasets

The first dataset was collected from the transcriptome of human wild-type TREM2 and isogenic TREM2-R47H DAM xenografted microglia (xMGs), isolated from chimeric AD mice [14]. The second dataset, integrated with xenografted microglia was collected from multimodal CRISPR-based genetic screens in human iPSC-derived microglia [15]. The third single-nuclei transcriptomic profiles of brains were collected from the Knight-ADRC and DIAN brain banks (WASHU) to enrich with the carriers of familial mutations causal of early onset familial AD (in *APP*, *PSEN1* and *PSEN2*), carriers of high-risk variants in TREM2, and sporadic non-carriers AD and controls. SnRNA-seq data preprocessing, clustering, and cell state annotation of this third dataset were described elsewhere [12]. The last dataset integrated into these three datasets was derived from the aged postmortem brain samples from the Religious Orders Study and Rush

Memory and Aging Project (ROSMAP) study [16]. Samples with a minimum of 10 cells were considered for further analysis.

Integration of cohorts

The selected four scRNA-seq data underwent a rigorous preprocessing pipeline, adhering to best practices in data normalization and integration. The merged expression matrix was normalized using the *SCTransform* protocol by Seurat Version 5.0.1 [17]. This function calculates a model of technical noise in scRNA-seq data using "regularized negative binomial regression" as described in [18]. We regressed out, during the normalization, the number of genes, the number of UMIs, and the percentage of mitochondria.

After extensive optimization of Seurat V5 integration methods we found Anchor-based CCA integration outperformed other methods. The principal components were calculated using the 3000 most variable genes, and the Uniform Manifold Approximation and Projection (UMAP) analysis was performed with the top 30 PCs. However, PC1 with high batch effects was excluded from downstream analysis. The clustering was done using a resolution of 0.3.

Sample and batch entropy by clusters

To evaluate the sample and batch effects in clustering, Shannon entropy was used to calculate individual cluster entropies (Eq. 1) [19], and the weighted sum was used to calculate overall clustering entropy (Eq. 2). The entropies were normalized by dividing each entropy value by the maximum entropy possible for each scenario (batch ($n = 4$) = −2; sample (n = 490) = −8.9).

$$H(i) = -\sum_{j \in K} p(i_j)\, log_2 p(i_j) \tag{1}$$

$$H = -\sum_{i \in C} H(i)\, \frac{N_i}{N} \tag{2}$$

Normalized pointwise mutual information

To quantify the association between the original transcriptional state labels with integrated clusters, normalized pointwise mutual information (NMI) was calculated for each cohort (Eq. 3). We normalized the NMI value between −1 to 1, where value of −1 indicates a complete absence of association between the original transcriptional state labels and integrated clusters, 0 denotes independence, and + 1 signifies a perfect alignment where each label consistently corresponds to a specific cluster, and vice versa. We used the svs version 3.0.0 to calculate NMI.

$$npmi(x;y) = \frac{pmi(x;y)}{h(x,y)} \tag{3}$$

Microglia transcriptional state differential expression

To determine if there was unique functionality of each integrated cluster, we fitted a linear mixed model that predicted the expression level of each gene for the individual nuclei by integrated cluster and corrected for the subject of origin and datasets (Eq. 4) [20]. Expression levels were extracted from the Seurat objects using *GetAssayData* with the 'slot' parameter set to "counts". The R package nebula (v1.5.1) [21] was used to implement the model, including parameters for a zero-inflated negative binomial distribution (model = "NBLMM", method = "LN") and the random effect of the subject of origin [21]. Within each microglia cluster, differential expression (DE) was calculated on each cluster versus all other.

$$\begin{aligned}&\text{Expression} \sim \text{Cluster} + (1|\text{Subject}); \text{ZI model} = \sim 1;\\ &\text{ZINB distribution}\end{aligned} \tag{4}$$

Pathway analyses

The upregulated genes (logFC > 0.25) identified for each integrated cluster were utilized in a subsequent pathway analysis employing the R-based application enrichR. For pathway enrichment, we utilized gene sets from either "KEGG 2021 Human" or "GO Biological Process 2021".

A heatmap was constructed to consolidate the upregulated "GO Biological Process 2021" (GO_BP) hits across all clusters. The -log10 P values for each GO_BP term within each cluster were combined into a single table. The top ten GO_BP terms with the highest averages of transformed P values across all clusters were then ranked. Subsequently, these terms were processed through rrvgo (v1.14.1), an R package implementing the Revigo [22] tool for summarizing GO_BP terms. The calculateSimMatrix function was employed to determine the relationships between the GO_BP terms, with parameters set as follows: orgdb = "org.Hs.eg.db", ont = "BP", method = "Rel". The terms were further summarized using reduceSimMatrix with the following specifications: score = "Rank", threshold = 0.6, orgdb = "org.Hs.eg.db". The summarized terms or "parentTerms" along with their corresponding *P*-values were then utilized to generate the heatmap. Row ordering was performed using the dist function with method = "euclidean", while column ordering utilized method = "p" for Pearson correlation.

Differential proportion analysis

We employed linear regression models testing each individual's cluster compositions to identify associations between microglia transcriptional states and disease

group. More explicitly, the number of nuclei a subject had in a specific cluster was divided by the subject's total nuclei count from clusters representing all cell types, creating a proportion.

The proportions were normalized using a cube root transformation and were corrected by disease status depending on the variable of interest. We removed participants without sample information. We utilized *glm*, a standard function in R, to implement the model (Eq. 5).

$$(\text{Proportion})^{1/3} \sim \text{AD status} \tag{5}$$

To visualize these results, cell state proportions were averaged between the samples in a group and displayed in a stacked barplot using the ggplot2 (v3.4.4) library in R.

Integration of snRNA-Seq and SRT data from human MTG

The 10X Genomics Visium data from the MTG of three Control (Braak stages I-II, male, aged 58, 72, and 82 years) and three AD (Braak stages III-IV, male, aged 86, 86, and 89 years) cases was collected [23]. We specifically chose the gray matter from three AD and Control donors for integration due to its direct relevance to AD pathology. The merged expression matrix of these AD and Control samples underwent normalization using the SCTransform protocol in Seurat Version 5.0.1, with parameters set to assay = "Spatial" and method = "poisson". Principal component analysis was conducted on the first 3000 variable genes, followed by UMAP analysis utilizing the top 12 principal components. Clustering was performed using default parameters (0.8). We employed 'Reference-based' integration method of Seurat V5 to integrate snRNA-seq and SRT dataset. Subsequently, using above mentioned four datasets we constructed an integrated reference comprising 222,822 single-cell nuclei of microglial transcriptional states. This integrated reference facilitated the analysis of conserved states across different conditions and brain regions. Given the pivotal role of microglia transcriptional states in AD etiology.

Validation of spatial segregation of Homeostatic and DAM states in FC

We selected SRT samples from the frontal cortex of AD, non-treated individuals from van Olst et al. (2025) [24] as a validation dataset for microglial spatial segregation. This dataset was generated using the same spatial technology as the MTG samples. We selected the highest-quality sample (GSM8184313) from van Olst et al., based on the median number of detected genes and UMIs per spot, to perform marker-based annotation of cortical layers. First, low-quality spots were removed using the 5th percentile threshold for both the number of UMIs and detected genes. Spot deconvolution was performed using cell2location (v0.1.4) [25] with default parameters and the SEA-AD reference atlas [26] to identify neuron-enriched spots, based on the 10th percentile of the inferred neuronal cell distribution. Normalization and spatial clustering followed the same protocol used for MTG SRT data preprocessing, and cluster markers were identified using the FindAllMarkers() Seurat function with default parameters. We intersected spatial cluster markers with established layer-specific markers [24], which resulted in high concordance between our cluster-based annotation and the manual annotation reported in the original study. This enabled classification of cortical regions as "External" (Layers I–III) or "Internal" (Layers IV–VI). Finally, our microglial atlas was projected onto this sample using the Seurat v5 reference-based integration method. We quantified the state enriched spots by selecting the ones within the top 25% probability for each DAM or Homeostatic states and compared their proportions in each cortical region using a Chi-square test in R.

Annotation of cortical layers and AD pathology-associated spots

To compare each integrated transcriptional states expression between cortical layers, we calculated the fraction by dividing the number of spots in a specific transcriptional state by the total number of spots in that cortical layer. This data was utilized to create a heatmap using the ggplot2 (v3.4.4) library in R.

Aβ plaques and AT8-tangles spots were categorized into proximal and distal levels based on their distance from Aβ and tau pathology respectively. All spots were previously manually annotated regarding the presence of Aβ plaques based on immunostaining from immediately adjacent tissue slices [23]. For the comparisons between Aβ-proximal versus distal spots, we defined as Aβ-proximal spots any spot that directly overlapped Aβ plaques, and others as Aβ-distal spots.

We identified and quantified each transcriptional state expression changes around these regions by selecting spots with the top 25% highest probability for each level. We conducted a Chi-square significance test in R to compare the fraction between levels. Specifically, we divided the number of spots in a specific transcriptional state by the total number of spots in that level to create a fraction. The results were visualized using bar plots created with the ggplot2 (v3.4.4) library in R.

Tissue processing and immunofluorescence stanning

Serial adjacent sections (10 µm each) of the MTG and fresh-frozen frontal lobe tissue were obtained from post-mortem human donors clinically diagnosed with AD. FFPE MTG sections were air-dried at 60 °C for 10 min, fixed and permeabilized in pre-chilled acetone (– 20 °C, 15 min), and subjected to antigen retrieval as previously

described [23]. Sections were blocked for 1 h at room temperature with 10% donkey serum in PBS and incubated overnight at 4 °C with primary antibodies: anti-Aβ (Ab2539, Abcam; 1:500) or anti-P2RY12 (848,002, BioLegend; 1:1000). Subsequently, sections were washed three times in 0.3% PBST, incubated with species-appropriate secondary antibodies for 2 h at 37 °C, and counterstained with DAPI. Autofluorescence was quenched using 0.5 × TrueBlack (Biotium) in 70% ethanol for 10 min. Quantitative comparisons of P2RY12 immunoreactivity between AD samples were performed using Student's t-test.

Fresh-frozen FC tissue fragment was embedded in Optimal Cutting Temperature (OCT) and cryosectioned at 10 µm. Two consecutive tissue sections were fixed in 3.7% formaldehyde and blocked in 2% bovine serum albumin (BSA) solution for 30 min. One section was co-immunostained for Aβ and phosphorylated-TAU (pSer202/pThr205) respectively using anti-Aβ (10,323, IBL; 1:1000) and anti-tau (SMC-601, StressMarq; 1:1000) primary antibodies. The adjacent section was stained for CD68, a marker of activated microglia, using a conjugated anti-CD68 antibody (AB_3251373, ThermoFisher; 1:10). Primary antibodies were incubated at room temperature for 1 h, followed by three washes in 0.3% PBST and secondary antibody incubation for 20 min in a 0.5 × DAPI solution. Prior to imaging, the autofluorescence was quenched using 1 × TrueBlack solution, as previously described.

CD68 immunofluorescence (IF) was analyzed using QuPath (v0.6.0) [27]. To quantify the prevalence of $CD68^{+}$ cells in internal and external cortical regions, we first defined a region of interest (ROI) spanning the full thickness of the gray matter, from the innermost to the outermost cortex. Nuclei were detected using DAPI staining with the cell detection tool from QuPath, applying default parameters except for an optimized intensity threshold of 30, which provided the most accurate nuclei segmentation, followed by cell expansion to define cell boundaries. $CD68^{+}$ cells were then identified by overlapping high-intensity CD68 IF signals with the detected cells. Cells with CD68 intensity above the average signal were classified as $CD68^{+}$. To determine cortical depth, we selected cells located at the inner and outer extremes of the ROI and used their positions to define a relative depth axis. All cells were projected onto this axis using min–max normalization, generating a continuous scale ranging from 0 (most internal) to 1 (most external). The distribution of $CD68^{\pm}$ cells was assessed in this relative depth scale.

Table 1 Demographic characteristics of samples

(a) Xenografted microglia					
Samples	Wild	TREM2			
Total	3	2			
Total #nuclei	17,769	7638			
(b) Human parietal cortex (WASHU)					
Samples	Control	ADAD	sAD	Presym	Other
Total	7	15	25	3	7
Total #nuclei	2784	3927	6048	544	2423
MS4A (AG)*	1665	1521	2951	167	334
PSEN1	-	12	-	-	-
TREM2	-	-	7	-	3
AOD (mean, sd)	92.14 (8.3)	52.64 (6.8)	81(8.84)	77.33 (15.28)	89.86 (5.64)
Sex (XY%)	40.05	48.28	53.95	30.7	30.13
PMI (mean, sd)	12.3 (5.51)	14.73 (8)	11.81(7.4)	12.42 (1.91)	13.87 (9.17)
(c) Human multiple region (ROSMAP)					
Sample	Control	EarlyAD	LateAD		
Total	220	133	74		
Total #nuclei	89,926	47,787	28,626		
AOD (mean, sd)	88.2(10.67)	87.57 (8.35)	87.86 (7.61)		
Sex (XY%)	51.72	50.03	34.28		
PMI (mean, sd)	15.33(16.52)	12.96 (9.4)	9.25 (5.98)		

*MS4A is referring to SNP rs1582763 (GG:25, AG:28, and AA:13)

Results

Building an atlas to discover the shared transcriptional diversity across human and iPSC-derived microglia atlas

To provide a comprehensive repertoire of microglia diversity in postmortem human brains and human cell based experimental models, we integrated single-cell and SRT dataset from multiple cohorts and brain regions. Table 1 provides a summary of the clinical, neuropathological, and experimental data of these datasets.

We integrate microglia from two in vitro models: The first experimental dataset involves Xenografted-microglia (xMGs) that represents seven distinct clusters of approximately 31,617 single cell nuclei [14]. Homeostatic, DAM, IFN, IL1B and MHCII transcriptional states were selected to be further integrated into the atlas, however clusters labeled "Degranulation" and "Humanin-like" were excluded due to their underrepresentation in human postmortem tissues. In this study, wild-type and R47H human microglial progenitors were transplanted into 5x-hCSF1 mice, to investigate how this mutation affects lipid droplet accumulation, and the microglial response to Aβ plaques. After seven months, GFP-expressing TREM2 and isogenic TREM2-R47H xMGs were extracted from the brains of 5x-hCSF1 mice and subjected to scRNA-seq [14]. Each cluster represents a unique microglial state for both TREM2 and TREM2-R47H xMGs [14] (Fig. 1a, Table 1a).

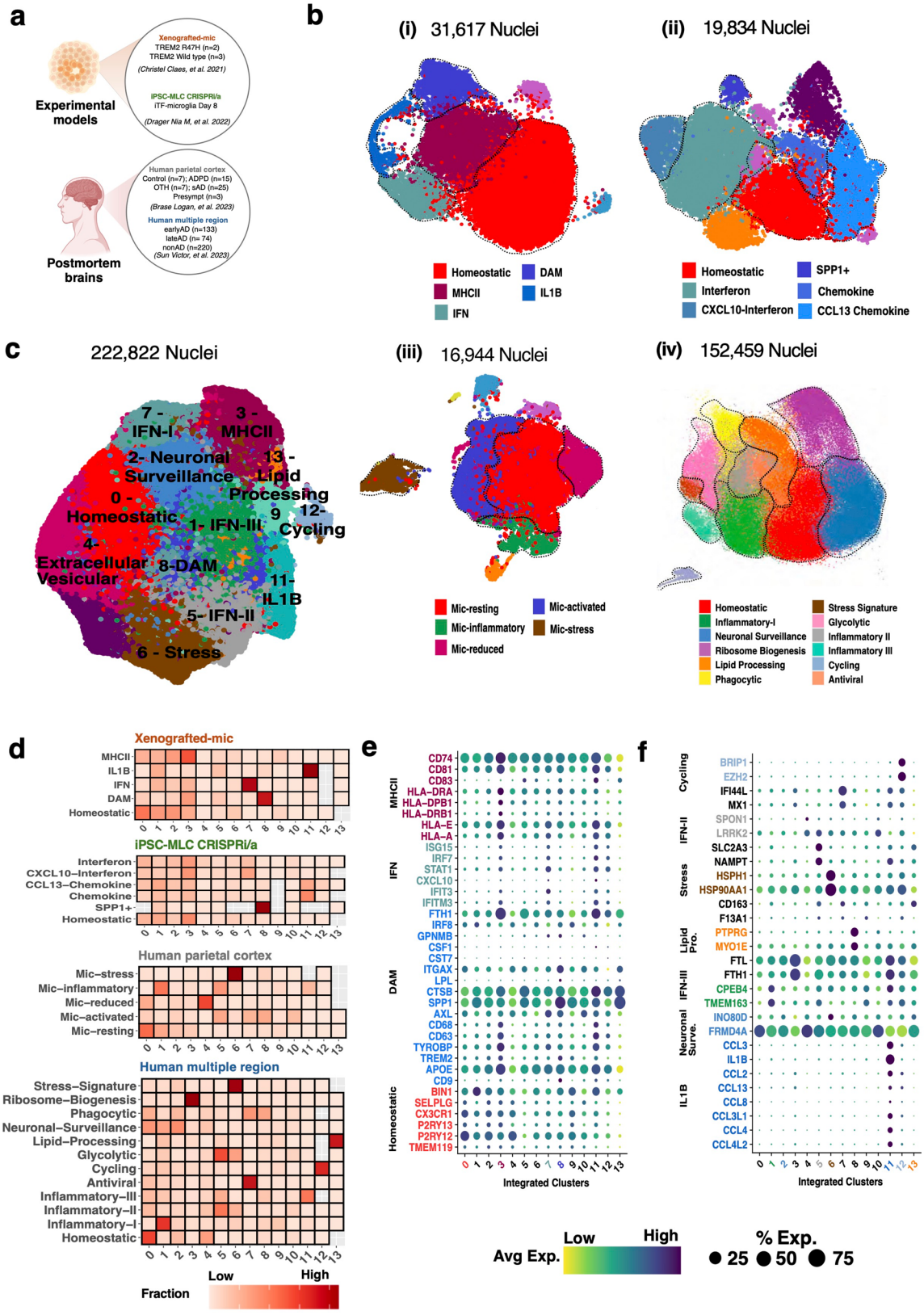

Fig. 1 (See legend on next page.)

(See figure on previous page.)

Fig. 1 Integration of Single-cell transcriptomics datasets. **a** Diagram depicting the single-cell transcriptomics dataset utilized. **b** Highlighted transcriptional states selected from each single-cell transcriptomics dataset, demarcated with dotted lines. **c** UMAP plot showing 14 distinct integrated clusters labeled 0–13, comprising a total of 222,822 cells. **d** Quantification of individual cell state contributions to the integrated transcriptional state. **e**–**f** Gene expression analysis within each transcriptional state, referencing studies by Yun Chen et al. [28] and Sun Victor et al. [16]. Cluster numbers and gene names are highlighted with the same color code to indicate enrichment. Note: Xenografted-mic term used for Xenografted-microglia

The second dataset included in this atlas was derived from multimodal CRISPR-based genetic screens in human iPSC-derived microglia (also named as iPSC-MLC CRISPRi/a) [15] (Fig. 1a). Unsupervised clustering and UMAP dimensional reduction of iPSC-MLC CRISPRi/a revealed nine transcriptionally distinct clusters for 19,834 nuclei [15]. Here, Homeostatic, SPP1 +, CXCL10-Interferon, Interferon, Chemokine and CCL13-chemokine were selected, although clusters associated with "Metallothioneins", "P53", and "Proliferative" signatures were excluded from the integrated atlas due to their underrepresentation in the postmortem human datasets.

Our atlas also integrated ex vivo data. We included microglia from postmortem human microglia from parietal cortex from our previous work [12]. We identified nine microglia transcriptional states for about 16,944 nuclei from 57 donors, including 15 carriers of pathogenic mutations in *APP* and *PSEN1* (autosomal dominant AD; ADAD), 25 sAD non-carriers. Clusters showing nucleus with lowest QC scores (namely mic-5, 6, 7, and 8) were exclude from WASU dataset. In addition, we included three individuals who matched AD-neuropathological criteria but without clinical cognitive impairment at death (presymptomatic), 7 individuals who matched non-AD neurodegenerative pathologies criteria (Other), and 7 individuals who exhibited neither neurodegenerative pathology nor evidence of dementia (Control) (Fig. 1a, Table 1b).

The fourth dataset includes 166,339 single microglia nuclei from aged postmortem brain samples of 427 individuals from the ROSMAP study [16]. This includes 207 AD donors (133 early and 74 late) and 220 nonAD individuals across six brain regions: prefrontal cortex (PFC), hippocampus, mid-temporal cortex, angular gyrus, entorhinal cortex, and thalamus. Here, we identified 12 distinct microglia transcriptional states (Fig. 1a, Table 1c).

We selected clusters that were sufficiently represented in each of the datasets (Fig. 1b), considering both the number of cells contained within each cluster and the extent to which these clusters fairly represented the diverse range of donors included in the study (Table 2). This selection process ensured that each cluster provided a comprehensive overview of the biological diversity present across the samples. By maintaining broad biological representation, we were able to maximize the significance and robustness of the integration, thereby enhancing the reliability and validity of our findings (Additional file 1). After comparing methods and optimizing parameters, we chose the Canonical Correlation Analysis (CCA) method implemented in the SeuratV5 package that high accuracy and exhibited minimal batch effects (Fig S1a-h). We integrated a total of 222,822 nuclei into 14 clusters that are represented in the four datasets (Fig. 1c). We confirmed that all samples and batches were adequately represented across the different clusters (Fig S2a-b).

We examined overlap exists between integrated cluster and transcriptional states of each cohort. Cells from all cohorts were reorganized while preserving their biological relevance. (Fig. 1d, see NMI in Methods: Fig S1). For instance, the majority of homeostatic cells from both in vitro and ex vivo were grouped into Cluster 0, stress-related cells from both ex vivo were found in Cluster 6 while DAM states from in vitro and the ex vivo parietal cortex cohort converged into Cluster 8. Although no DAM cluster was clearly identified in the Human multiple region (ROSMAP) samples [16], by virtue of aggregating multiple dataset we were able to reassign few nuclei to the DAM cluster (Fig. 1d). Finally, to evaluate the association of transcriptional states to amyloid plaques and tau tangles, we selected SRT datasets from human Middle Temporal Gyrus (MTG) AD samples ($N = 3$) and Control ($N = 3$) generated using the 10X genomics Visium platform.

Characterization of integrated transcriptional states

We annotated the 14 integrated clusters based on their molecular signatures and functions, utilizing well-known canonical standard markers for Homeostatic, DAM, IFN, and MHCII [28] (Additional file 2). We expanded this list by incorporating additional representative markers from Sun et al. (2023) [16] for newly reported transcriptional states. We identified an average of 941 upregulated genes (FDR < 0.05) for each transcriptional state, revealing a rich transcriptional diversity within all integrated transcriptional states (Additional file 3).

Homeostatic microglia (Cluster 0) were characterized by high expression of well-known homeostatic markers such as P2RY12 (log2FC = 0.28, adj. $p = 7.73 \times 10^{-504}$), P2RY13 (log2FC = 0.21, adj. $p = 5.24 \times 10^{-131}$), and CX3CR1 (log2FC = 0.19, adj. $p = 9.23 \times 10^{-165}$) (Fig. 1e, Additional file 3). DAM microglia (Cluster 8) exhibited higher expression of SPP1 (log2FC = 1.45, adj. $p = 7.97 \times 10^{-3290}$), LPL (log2FC = 1.93, adj. $p = 3.40 \times 10^{-578}$), CD9 (log2FC = 1.83, adj. $p = 2.27 \times 10^{-1331}$), TREM2 (log2FC = 0.59, adj.

Table 2 Distribution of microglia across cohorts

	Xenografted microglia	iPSC-MLC CRISPR i/a	Human parietal cortex	Human multiple region
Total # nuclei	31,617	19,834	16,944	166,339
Total # nuclei selected*	25,407	15,350	15,726	166,339
Transcriptional states selected[@]	5/7	6/9	5/9	12/12
Mean # genes	1459	3382.76	1815.266	1634
Mean #UMI	2926	11,069.8	3398.226	2993.9
Avg % mitochondria	4.912	3.03148	0.99792	0.8811

*Samples were removed if they don't have at least ten nuclei

#Number

@selected transcriptional states are mentioned in Additional file1

$p = 1.50 \times 10^{-511}$), and CD68 (log2FC = 0.29, adj. $p = 8.04 \times 10^{-74}$) [29] (Fig. 1e, Additional file 3).

In MHCII (Cluster 3), we observed higher expression of HLA-A (log2FC = 0.22, adj. $p = 1.52 \times 10^{-182}$), HLA-E (log2FC = 0.08, adj. $p = 4.57 \times 10^{-42}$), and HLA-DPB1 (log2FC = 0.64, adj. $p = 6.17 \times 10^{-529}$) and marker genes associated with "positive regulation of lymphocyte proliferation" (adj. $p = 1.75 \times 10^{-2}$) (Fig. 1e, Additional file 3 and 4).

We identified three inflammatory states showing high expression of IFN-induced gene (Clusters1, 5, and 7). Cluster 7 showed overexpression of IFIT3 (log2FC = 1.57, adj. $p = 1.37 \times 10^{-1418}$) (Fig. 1e, Additional file 3), and showed strong functional enrichment in immune responses, including defense response to virus (adj. $p = 7.45 \times 10^{-20}$), and cytokine-mediated signaling pathway (adj. $p = 2.77 \times 10^{-11}$) (Additional file 4). We also found TMEM163 (log2FC = 0.52, adj. $p = 9.82 \times 10^{-483}$) in Cluster 1 and LRRK2 (log2FC = 0.36, adj. $p = 1.45 \times 10^{-125}$) in Cluster 5 (Fig. 1f, Additional file 3).

We observed significant enrichment of stress markers such as HSP90AA1 (log2FC = 1.73, adj. $p = 5.92 \times 10^{-6228}$) and HSPH1 (log2FC = 1.56, adj. p = 3.21×10^{-3248}) related to the regulation of cellular response to heat (adj. $p = 3.23 \times 10^{-8}$) in Cluster 6 (Fig. 1f, Additional file 3 and 4). Interleukin IL1B (log2FC = 3.70, adj. $p = 8.41 \times 10^{-2568}$) and CCL4 (log2FC = 4.82, adj. $p = 1.31 \times 10^{-1480}$) and additional genes related to the "cytokine-mediated signaling" (adj. $p = 2.29 \times \times 10^{-10}$) were overexpressed in Cluster 11 (Fig. 1f, Additional file 3 and 4).

Cluster 4 showed expression of SPARC (log2FC = 0.51, adj. $p = 1.27 \times 10^{-55}$) (Fig. 1e, Additional file 3), and strong functional enrichment of extracellular structure organization (adj. $p = 2.68 \times 10^{-6}$), external encapsulating structure organization (adj. $p = 2.68 \times 10^{-6}$), extracellular matrix organization (adj. $p = 5.64 \times 10^{-4}$), and ECM-receptor interaction (adj. $p = 8.17 \times 10^{-4}$), henceforth designated as Extracellular Vesicular (EV) microglia (Additional file 4). And Cluster 2 exhibited high expression of neurotransmitter receptors related to cell–cell junction organization (adj. $p = 2.73 \times 10^{-3}$) (Fig. 1f, Additional file 4), while we identified Cluster 12 as a cycling state due to the enrichment in DNA metabolic process (adj. $p = 2.42 \times 10^{-31}$) (Fig. 1f, Additional file 4). We annotated Cluster 13 as a lipid-processing state based on the enrichment of representative marker TPRG1 (log2FC = 1.20, adj. $p = 9.96 \times 10^{-19}$) (Fig. 1f, Additional file 3). We did not find any specific functional enrichment in clusters 9 and 10, neither were those nuclei flagged by our quality control process. Therefore, we labeled them as Unknown (Fig. 1e-f, Additional file 3).

Furthermore, we examined the expression of each marker gene in each dataset (Fig. 2a and Fig S3), to verify they were consistently expressed. We also calculated pairwise pearson correlations between the log fold-changes (logFC) of all differentially expressed genes (logFC > 0.25, P < 0.05) from each cohort microglia subtype and our integrated microglial clusters. We found high degree of concordance between our integrated transcriptional state and each cohort transcriptional state indicating that key transcriptional features are bioconserved (Additional file 5). Our analysis revealed consistency in gene expression patterns across all datasets, further enhancing the reliability and generalizability of our insights. Based on strong evidence of gene expression and proportional analysis, Clusters 0, 3, 8, 6, and 11 were classified as Homeostatic, MHCII, DAM, Stress, and IL1B. IFN-I, IFN-II, and IFN-III cells were identified in clusters 7, 5, and 1. Clusters 2, 4, 12, and 13 were annotated as Neuronal Surveillance, extracellular vesicular, Cycling, and Lipid Processing respectively (Fig. 1c). The biological pathway analysis of each annotated transcriptional state is shown in Additional file 6.

Relative proportions of microglia transcriptional states across AD groups

To evaluate whether the relative proportions of these transcriptional states change in AD groups, we tested the statistical significance of cell fractional differences between control and other individuals, including those in ex vivo datasets and in Xenografted-microglia with AD risk variants in *TREM2* and wildtype (Fig. 2b, Additional file 7).

A prominent Stress cell state was enriched in ADAD samples from the Human parietal cortex (WASHU) cohort ($\beta = 0.30$, $p = 1.67 \times 10^{-2}$; Fig. 2b, Additional file 7). The Gene Ontology analysis revealed its association with "regulation of cellular response to heat" (adj. $p = 3.29 \times 10^{-8}$), "chaperone cofactor-dependent protein refolding" (adj. $p = 1.15 \times 10^{-7}$) and "regulation of inclusion body assembly" (adj. $p = 6.19 \times 10^{-4}$) (Fig. 2c, Additional file 8). These nuclei overexpressed HSP90AA1 and HSPH1 genes, suggesting these play a role in synaptic

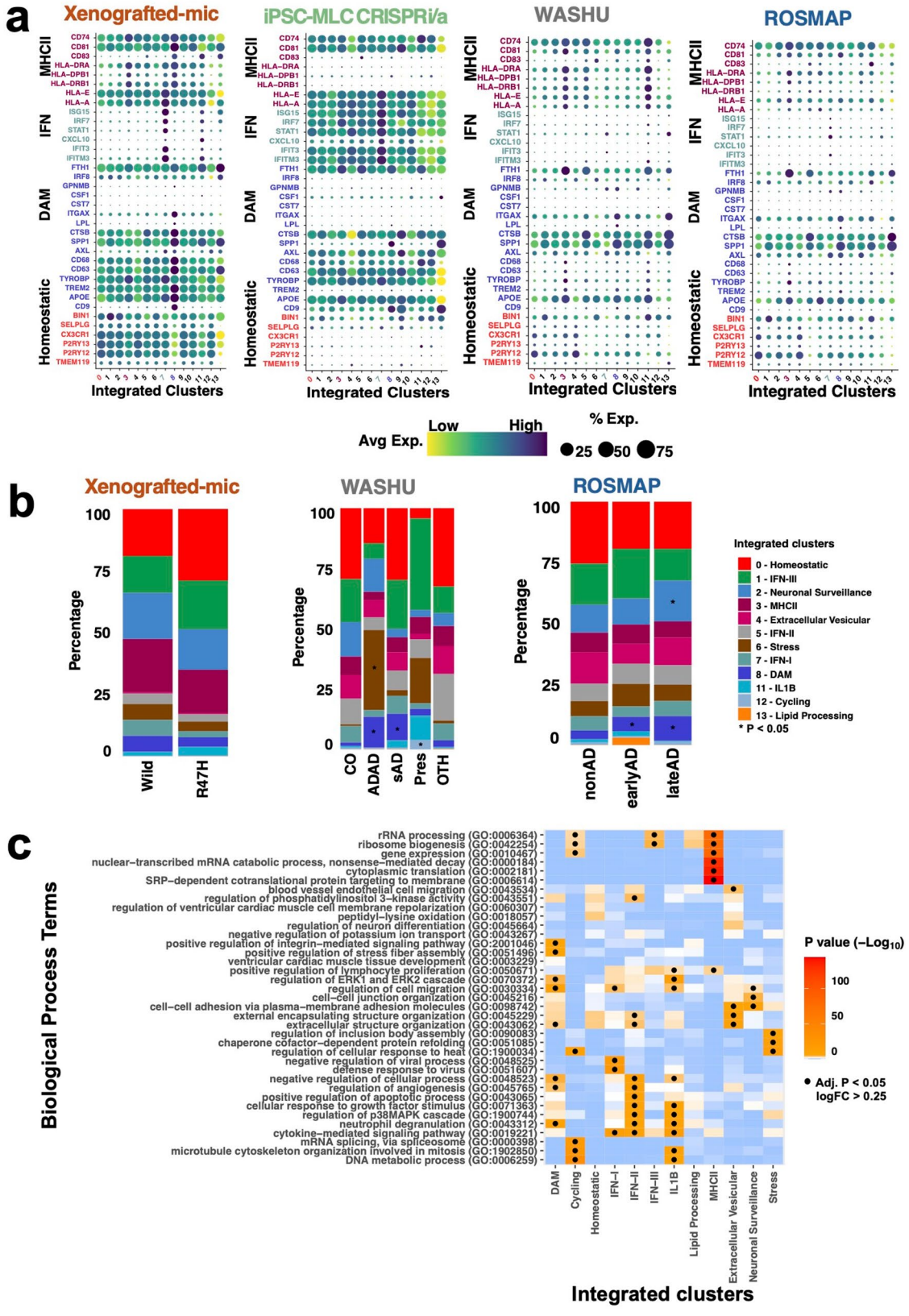

Fig. 2 (See legend on next page.)

(See figure on previous page.)

Fig. 2 Biological conservation of functionality across diverse populations or conditions. **a** Analysis of canical marker gene expression within each integrated cohort. Cluster numbers and gene names are highlighted with the same color code to indicate enrichment. **b** Proportion plots illustrating the enrichment of specific transcriptional states in Control participants compared to all other participants across each cohort. Proportions were calculated for each sample (see Methods). For visualization, sample proportions are averaged by sample status. (*) denotes significant ($p < 0.05$) enrichment of that cluster within samples, as determined by linear regression. Exact p-values can be found in the Supplementary Dataset. ADAD: Autosomal Dominant Alzheimer's Disease, sAD: Sporadic Alzheimer's Disease, Pres: Presymptomatic, CO: Neuropathology-free, OTH: Non-Alzheimer's Disease Neurodegenerative. **c** Heatmap displaying enriched pathways within the upregulated genes for each transcriptional state. Differentially Expressed Genes (DEGs) were identified from linear mixed models comparing each transcriptional state to all other states. Gene Ontology (GO) Biological Process terms were summarized and selected as described in the Methods. (·) indicates a significant (Benjamini–Hochberg adjusted $p < 0.05$) association, as calculated by the R package enrichR. Exact p-values can be found in the Source Data file. Note: Xenografted-mic term used for Xenografted-microglia

homeostasis and Aβ pathology, as previously observed in the entorhinal cortex in AD patients [30]. In the case of Human multiple regions (ROSMAP) we did not find significant enrichment of Stress transcriptional state in AD groups comparison to control.

Both ex vivo datasets exhibited enrichment of DAM transcriptional states in AD groups, but such association was not significant in the Xenografted TREM2-R47H samples. The DAM transcriptional state was specific to ADAD ($\beta = 0.23$, $p = 1.78 \times 10^{-3}$; Fig. 2b, Additional file 7), and sporadic AD ($\beta = 0.19$, $p = 5.53 \times 10^{-3}$; Fig. 2b, Additional file 7) in the Human parietal cortex (WASHU), similarly in the earlyAD ($\beta = 0.12$, $p = 9.44 \times 10^{-12}$; Fig. 2b, Additional file 7) and late AD ($\beta = 0.19$, $p = 9.81 \times 10^{-17}$; Fig. 2b, Additional file 7) from the Human multiple region (ROSMAP) cohort. Several experimental models support that in response to Aβ pathology, microglia cells proliferate and acquire a DAM transcriptional profile [31–33]. However, excessive microglia activation may exacerbate neuronal damage at later stages of amyloid pathology [31, 34–36]. A gene ontology analysis reveals that DAM cells are associated with the regulation of cell migration ($p = 1.67 \times 10^{-4}$), regulation of ERK1 and ERK2 cascade ($p = 1.18 \times 10^{-2}$), and positive regulation of stress fiber assembly ($p = 2.61 \times 10^{-3}$) (Fig. 2c, Additional file 8). Additional studies support that the ERK1/2 pathway governs inflammatory cytokine production and iNOS expression in DAM, highlighting its importance in neuroinflammatory processes and as a potential therapeutic target [37]. Additionally, activation of the Rho/ROCK signaling pathway boosts stress fiber assembly in microglia, facilitating essential cytoskeletal rearrangements for phagocytosis and activation [38, 39].

The Cycling transcriptional state was enriched in Presymptomatic individuals (general linear regression $\beta = 0.19$, $p = 1.86 \times 10^{-2}$; Fig. 2b, Additional file 7) from the Human parietal cortex (WASHU). Biological pathway analysis revealed associations of the Cycling transcriptional state with the DNA metabolic process ($p = 2.42 \times 10^{-31}$), microtubule cytoskeleton organization involved in mitosis ($p = 1.12 \times 10^{-19}$), and mRNA splicing via spliceosome ($p = 1.32 \times 10^{-16}$) (Fig. 2c, Additional file 8). These findings suggest a potential role for these pathways in driving microglial proliferation, implicating their involvement in the early stages of neuroinflammatory processes associated with AD.

Neuronal surveillance cells were enriched in late onset AD (general linear regression $\beta = 0.06$, $p = 2.06 \times 10^{-2}$; Fig. 2b, Additional file 7) samples from multiple region cohorts, showing it significant involvement in "cell–cell adhesion via plasma-membrane adhesion molecules" ($p = 9.00 \times 10^{-4}$), "cell–cell junction organization" (GO:0045216) ($p = 2.73 \times 10^{-3}$), and "regulation of cell migration" ($p = 4.52 \times 10^{-2}$) (Fig. 2c, Additional file 8). These processes suggest a potential role in modulating immune cell infiltration, microglial activation and possibly involvement in the blood–brain barrier integrity, highlighting them as potential therapeutic targets for mitigating neuroinflammation in AD [40–43]. However, we did not include the iPSC-MLC CRISPRi/a in Fig. 2b because the original study didn't expose these cells to any AD-relevant stimulus.

Benchmarking the microglial atlas by adding additional experimental iPSC-derived data

We integrated single-cell data from developmentally patterned models [44], to determine how well the atlas extends to iPSC-derived microglia models.

We conducted a comparative analysis between our integrated microglial clusters and stem-cell-differentiated microglia (iMGLs). Using the Seurat V5 label transfer we were able to annotate the 56,454 iMGLs (cell scores are shown in Additional file 9). We found an overlap between microglia states in Dolan et al. (2023) [44] and our reference predicted model (Fig. S4). Nuclei originally clustered and annotated as Antigen-presenting were predicted as MHCII (30.16%); similarly, DAM nuclei were predicted as DAM (22.10%). Interferon-responsive nuclei were predicted as Inflammatory-II (15.13%), proliferation nuclei as Cycling (58.46%), Transition nuclei as MHCII (26.10%), and neuronal-surveillance nuclei as Neuronal Surveillance (25.73%). Notably, a very small proportion of cells were predicted to match the Homeostatic microglia state, which aligns with expectations from in vitro models. These results suggest that our reference captures a wide range of microglial activation states that are present in longer-term differentiation models.

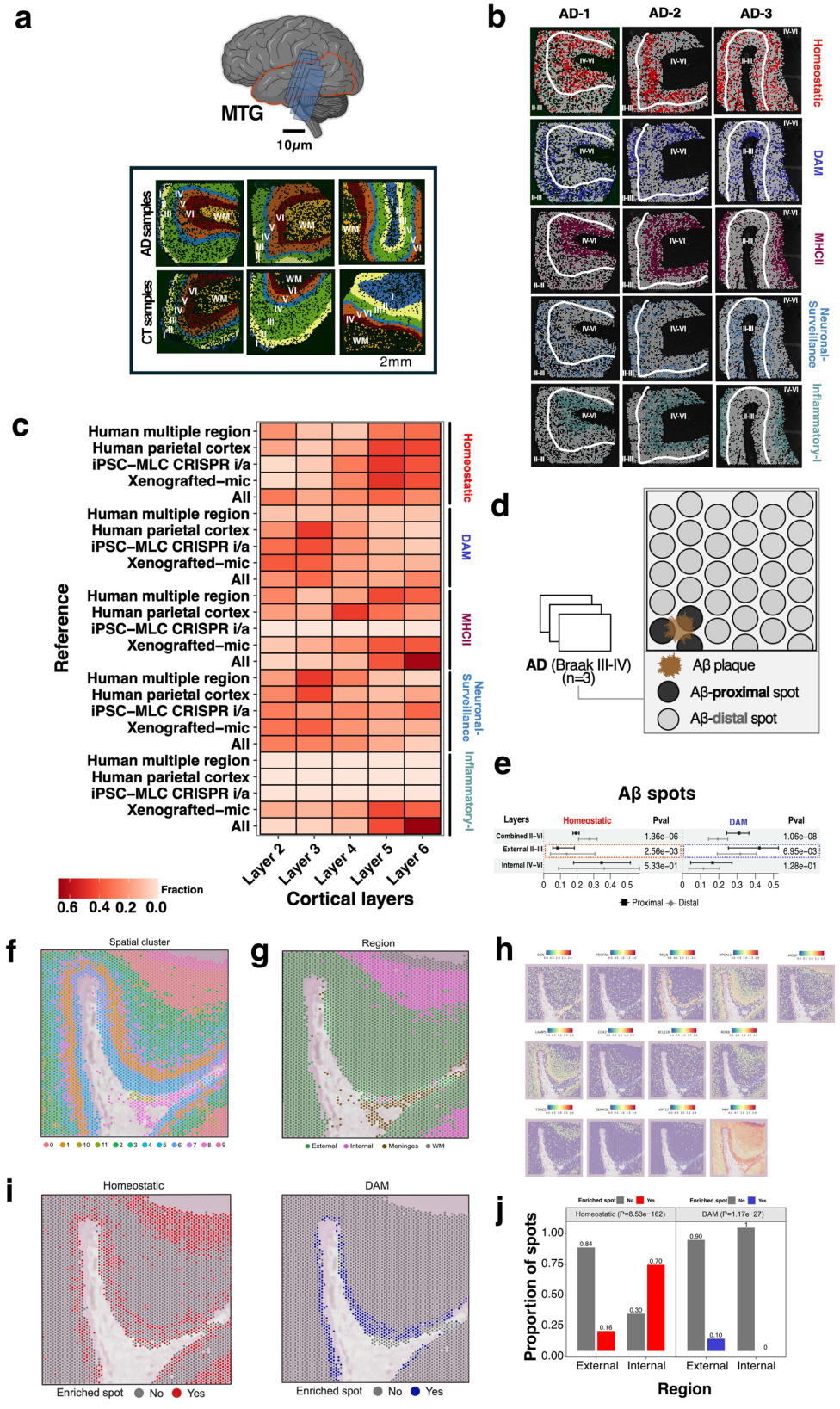

Fig. 3 (See legend on next page.)

(See figure on previous page.)

Fig. 3 Microglial transcriptional shift in response to AD pathology. **a** Spatial transcriptomics (SRT) of the Middle Temporal Gyrus (MTG) in Alzheimer's disease (AD), with each section being 10 µm thick. **b** Visium spots highlighting the top 25% highest probability for Homeostatic, DAM, MHCII, Neuronal Surveillance and Inflammatory-I states. **c** Heatmap illustrating the fraction of predicted transcriptional states within each cortical layer. **d** Overview of spatial transcriptomics Aβ localization. Aβ-proximal spots refer to those directly overlapping Aβ plaques, while all others are considered Aβ-distal. **e** Upper: Quantification of transcriptional states around proximal and distal Aβ spots for Combined II-VI, External II-III, and Internal IV-VI cortical layers. **f**-**j** SRT sample from AD frontal cortex from van Olst et al. [24]. f Spatially resolved clusters based on gene expression from van Olst et al. AD sample. **g** Cortical layers identified based on main layer markers reported in van Olst et al., shown in panel **h**. The grey matter layers were identified as External (Layers I-III) and Internal (Layers IV-VI). Meninges and white mater were not considered in the analysis. **i** The Homeostatic and DAM enriched spots identified across the grey matter. **j** Proportion of Homeostatic and DAM enriched spots in each Internal and External layers. Chi-square significance tests were used to calculate p-values (refer Fig. S9 for other transcriptional states). Note: Xenografted-mic term used for Xenografted-microglia

Microglial transcriptional shift in response to AD pathology

We sought to investigate the anatomical and neuropathological transcriptional distribution of single-cell microglia atlas. To do so, we integrated SRT datasets from human MTG AD samples ($N=3$) and Control ($N=3$) generated using 10X genomics Visium SD platform [23]. We selected those spots characterizing the cortical layers II to VI obtaining a total of 7,884 spots in AD and 5,976 spots in CT samples. As few spots were captured for layer I in AD samples, we removed those from our analyses. Then we integrated this data with the scRNA-seq datasets [12, 14–16] to investigate the distribution of microglia transcriptional states among cortical layers (Fig. 3a) and their proximity to AD pathological lesions (Aβ or NFTs). To do so, we conducted a reference-based integration to deconvolve and assign scores to each spot based on the resemblance of microglial transcriptional states. In our analysis, we focused on the highly predicted (top 25%) Visium spots for each sample, examining the distribution of each integrated reference transcriptional states across cortical layers (AD: Fig S5 and Control: Fig S6) and dataset (Fig S7). We observed a significant increase in spots capturing DAM in the external cortical layers II-III ($p=2.20e\text{-}16$), while internal layers IV-VI showed an increase in Homeostatic microglia ($p<2.2e\text{-}16$) (Fig. 3c, Additional file 10). We determined that this observation was not attributable to the presence of Aβ or NFTs. We observed this specific distribution of Homeostatic microglia from each of the dataset included in our atlas. Furthermore, we observed increased distribution of the DAM when we mapped each of the datasets, with the exemption of the Human multiple regions (ROSMAP) study (Additional file 10), possibly because this study did not capture sufficiently large number of DAM [16]. The MHCII transcriptional state showed a significant enrichment in the internal cortical layers in AD samples across multiple cohorts ($p=2.03\times10^{-238}$), and was not dataset specific (Xenografted microglia ($p=5.81\times10^{-108}$), Human parietal cortex ($p=9.35\times10^{-53}$), and Human multiple region ($p=1.86\times10^{-97}$)) with the exception of the iPSC-MLC CRISPR i/a model. The Neuronal Surveillance microglia state was predominantly enriched in the outer cortical layers of AD samples across datasets ($p=3.36\times10^{-43}$, Xenografted microglia ($p=1.49\times10^{-77}$), iPSC-MLC CRISPR i/a ($p=2.44\times10^{-3}$), Human parietal cortex ($p=1.94\times10^{-141}$), and Human multiple region ($p=2\times10^{-163}$)). The Inflammatory-I microglial state was significantly enriched in the inner cortical layers of AD samples ($p=1.66\times10^{-292}$) but only showed significance in Xenografted microglia dataset ($p=1.74\times10^{-96}$). In the control SRT data, a small fraction of cells exhibited a DAM signature, and DAM from the Xenografted microglia showed enrichment in the outer cortical layers across ($p=6.32\times10^{-30}$), as did the ones from the iPSC-MLC CRISPR i/a ($p=1.46\times10^{-62}$), and Human parietal cortex ($p=8.49\times10^{-47}$) datasets (Fig. S6, Additional file 10). Homeostatic microglia population was enriched in the inner cortical layers across all datasets ($p=3.81\times10^{-304}$) as well as specifically within the Human parietal cortex ($p=1.16\times10^{-238}$). Single-cell MHCII microglia state also showed enrichment in the inner cortical layers of SRT from control brains ($p=2.04\times10^{-221}$) but only showed significance in the Human multiple region dataset ($p=6.38\times10^{-182}$). In contrast, the Neuronal Surveillance microglia were enriched in the outer cortical layers of control brains ($p=9.96\times10^{-74}$; Xenografted microglia ($p=3.71\times10^{-31}$), iPSC-MLC CRISPR i/a ($p=8.49\times10^{-47}$), Human parietal cortex ($p=7.49\times10^{-18}$), and Human multiple region ($p=2.55\times10^{-106}$)).

Mapping single-cell transcriptional states to AD neuropathology

Generation of single-cell using 10X genomics or similar technologies requires the tissue dissociation, precluding the study of the relationship of transcriptional states to AD neuropathological lesions. Thus, we leverage the single-integrated cell and STR data to study relationship of transcriptional states in relation to the proximity of amyloid plaques (identified using Rabbit anti-Aβ antibody) and NFTs (identified using Human/murine phospho-tau pSer202/Thr205 antibody) in the human brain (Fig. 3d). We found that spots proximal to plaques (< 55 microns) tended to show DAM ($p=1.06\times10^{-8}$) and Neuronal Surveillance ($p=2.02\times10^{-9}$) microglia states, while distal spots showed a predominance of Homeostatic ($p=1.36\times10^{-6}$) and MHCII ($p=9.68\times10^{-5}$) microglial expression. The presence of the microglial disease

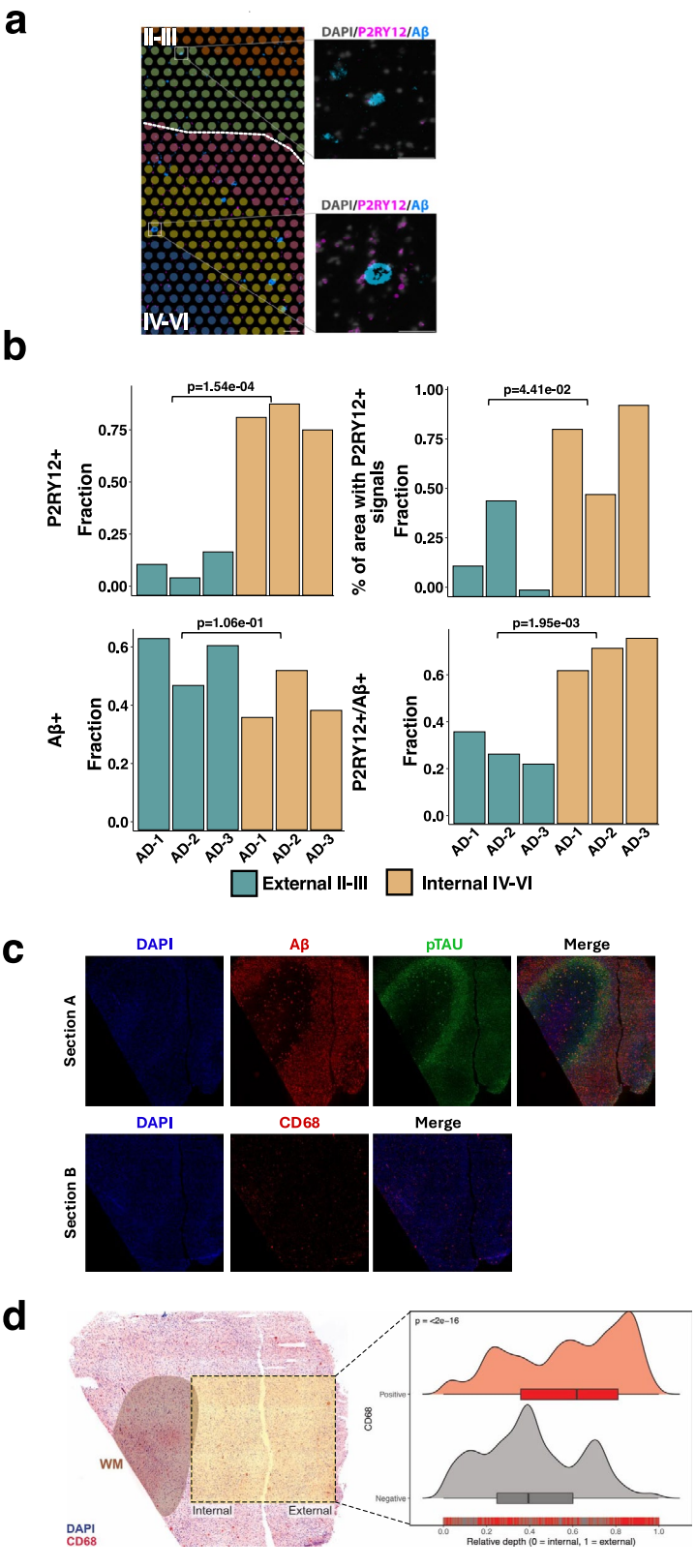

Fig. 4 (See legend on next page.)

(See figure on previous page.)

Fig. 4 Spatial distribution of microglial activation across cortical layers in Alzheimer's disease (AD) brain. **a** Immunofluorescence (IF) staining of P2RY12 and Aβ on adjacent Sects. (10 µm interval) from the Middle Temporal Gyrus of an AD donor, aligned to 10X Genomics Visium spatial transcriptomics spots (color-coded) across cortical layers II–VI (Chen et al., ANC, 2022) [23]. High-magnification images show nuclei (DAPI, gray), homeostatic microglia (P2RY12, magenta), and Aβ plaques (blue) in external layers II–III (top) and internal layers IV–VI (bottom). **b** Quantification of IF-stained P2RY12$^+$ cells and Aβ$^+$ plaques across cortical layers II–III and IV–VI in AD samples. Bar plots display normalized counts for: Upper Left—P2RY12$^+$ cells; Upper Right—Aβ$^+$ plaques; Lower Left—P2RY12$^+$/Aβ$^+$ overlap; Lower Right—P2RY12$^+$/Aβ$^-$ plaques. Counts were normalized to the total number within layers II–VI. **c** IF co-staining of Aβ (red) and phosphorylated tau (pTAU, green) in frontal cortex sections with AD pathology (Section A). Nuclei stained with DAPI (blue). Adjacent section (Section B) stained for CD68 (red), a marker of activated microglia. **d** Quantification of CD68$^+$ cells across cortical layers in AD frontal cortex. Graph shows distribution of CD68$^+$ and CD68$^-$ cells in external versus internal layers

associated ($p = 6.95 \times 10^{-3}$) and neuronal-surveillance ($p = 1.65 \times 10^{-3}$) states in proximity to amyloid plaques were predominantly observed in external cortical layers II and III while the Homeostatic ($p = 2.56 \times 10^{-3}$) was predominantly observed distal to amyloid plaques in external cortical layers II and III (Fig. 3e, Fig S8, Additional file 11). Notably, no such distinction was observed in relation to proximity of amyloid plaques in Inflammatory-I and NFT (Fig S8), although MHCII showed marginal association ($p = 9.27 \times 10^{-2}$).

To ensure that our observations were not driven by a single AD sample and/or limited to integrated data, we examined the distribution of transcriptional states across all AD samples using each cohort as a reference (Fig S9, Additional file 11). We found a prevalence of DAM near amyloid plaques, and the Homeostatic state was predominantly observed distal to amyloid plaques in each sample (Fig. 3e, Additional file 11). Importantly, this distribution pattern was not driven by differences in the burden of amyloid plaques among cortical layers.

To study other cortical regions, we analyzed SRT from the FC of an AD donor from from van Olst et al. (2025) [24]. We identified the cortical layers based on the gene expression of the layer makers (Fig. 3f-h). The spatial segregation of DAM and Homeostatic microglia was also observed in this sample (Fig. 3i-j), suggesting that this pattern of spatial differentiation can occur in different brain locations.

Immunohistochemistry data shows homeostatic and DAM distributions predicted by transcriptional data

To validate transcriptional findings, immunohistochemistry was performed on adjacent 10 µm sections of the human Middle Temporal Gyrus (MTG), matching the thickness used for Visium spatial transcriptomics [23]. Sections were stained for P2RY12, a purinergic receptor selectively expressed by homeostatic microglia, to map their distribution and assess microglial activity. To examine the spatial relationship between homeostatic microglia and amyloid-β (Aβ) plaques, the same section was co-stained for Aβ (Fig. 4a). Hematoxylin and eosin (H&E) staining of Visium gene expression sections revealed that both the distribution of P2RY12$^+$ cell counts ($p = 1.54 \times 10^{-4}$) and the percentage of cortical area occupied by P2RY12$^+$ signals ($p = 4.41 \times 10^{-2}$) were significantly higher in internal cortical layers IV–VI compared to external layers II–III, consistent with patterns observed in single-cell and SRT datasets (Fig. 4b; Additional file 12). The distribution of Aβ plaques ($p = 1.06 \times 10^{-1}$) and the spatial overlap between P2RY12$^+$ cells and Aβ plaques ($p = 1.95 \times 10^{-3}$) across cortical layers further confirmed that this enrichment was not driven by amyloid pathology (Fig. 4b; Additional file 12). Similarly, we performed additional immunohistochemistry on two consecutive sections of post-mortem human frontal lobe to assess microglial activation across cortical layers in the context of AD pathology (Fig. 4c-4d). One section was co-stained for Aβ and phosphorylated tau (pTAU), two established AD biomarkers (Fig. 4c, Section A), while the adjacent section was immunostained for CD68 (Fig. 4c, Section B), a marker of activated microglia (Fig. 2a) and overexpressed in DAM (log2FC = 0.29, adj. $p = 8.04 \times 10^{-74}$). Quantitative analysis of CD68$^+$ cells revealed an enrichment of activated microglia within external cortical layers of the frontal lobe (Fig. 4d), also corroborating spatial patterns observed in integrated single-cell and spatial transcriptomics datasets.

Discussion

The integration of single-cell and SRT data from various cohorts and brain regions has provided a comprehensive repertoire of microglia diversity in postmortem human brains and human cell-based experimental models. Single-cell technologies have been critical to study the alternative microglia transcriptional states in AD. However, because of the tissue dissociation processes needed to generate this data, the spatial and contextual information of the cells is not captured by these technologies, and thus the distribution of microglia across different brain regions is still not fully understood.

This study highlights the importance of considering the multifaceted nature of microglial dynamics in AD [45]. We harnessed data from different in vitro models, including xenografted-microglia and human iPSC-derived microglia, and integrating it with ex vivo human microglia from the ROSMAP study and parietal cortex samples, to create a microglial transcriptional atlas. This approach has enabled the identification of distinct microglial states associated with Homeostatic, DAM, IFN-mediated, and MHCII-expressing states across datasets.

However, the literature is limited in exploring how these varying transcriptional states correlate with Aβ plaques and NFTs, and how this relationship may differ across regional or cortical areas. Our findings reveal significant alterations in microglial transcriptional states in regions associated with AD pathology, particularly exacerbated in cortical layers II and III. This regional specificity underscores the nuanced interplay between microglial states and AD pathology and cerebral cortex anatomy. DAM and Neuronal Surveillance microglial states were predominantly localized to the outer cortical layers, whereas Homeostatic, MHCII and Inflammatory-I states were more prevalent in the inner cortical layers. This distribution pattern was consistent across all AD samples, indicating a robust association between microglial states and cortical layer-specific pathology.

Furthermore, our study uncovered intriguing associations between microglial states and Aβ plaque proximity. To the best of our understanding, this is the first study to show that regions proximal to Aβ plaques exhibited higher DAM and Neuronal Surveillance microglia in human brains, whereas distal regions displayed a prevalence of Homeostatic, and MHCII states. Numerous murine and xenotransplanted human microglia studies have also identified DAM—typically localized around Aβ plaques [46–48] which is characterized by the downregulation of homeostatic microglial genes (e.g. P2ry12, Tmem119, Cx3cr1) [46, 49] and the upregulation of genes involved in lipid metabolism, phagocytosis, and Aβ-related signaling (e.g. Apoe, Clec7a, Trem2) [46, 47]. Beyond the DAM profile, further transcriptomic studies have delineated additional Aβ-responsive microglial states, including activated response microglia (ARM) [50], interferon response microglia (IRM) [50], and MHC-II [51]. The IRM state is enriched for interferon-stimulated genes (e.g. Ifit3, Ifitm3, Irf7) and appears in amyloidosis models such as 5 × FAD, often in proximity to plaques and associated with synapse loss [47, 50]. This reinforces the translational relevance of murine and xenotransplant models and emphasizes the consistency of plaque-associated microglial responses.

This spatial relationship suggests a dynamic microglial response to Aβ pathology, where microglia near plaques are more likely to be in a disease-associated state, potentially phagocytosing Aβ but also contributing to local neuroinflammatory processes. The elucidation of diverse transcriptional states of microglia and their spatial distribution in relation to AD pathology provides valuable insights into the complexity of microglial responses in neurodegenerative diseases. In this initial attempt, the limited number of spatial transcriptomics samples may restrict the generalizability of our findings, but it provides a valuable starting point for researchers to explore this direction further. In line with prior studies [5, 52, 53], our finding suggest that regional microglial heterogeneity may reflect or contribute to the brain's differential vulnerability to pathological processes.

Conclusion

This work significantly contributes to our understanding of microglial activity in Alzheimer's disease. By integrating single-cell and SRT datasets, we have provided a detailed atlas of microglial diversity, revealing the regional and pathological specificity of microglial states. The study underscores the importance of considering the multifaceted nature of microglial dynamics in neurodegenerative diseases and highlights regional heterogeneity of microglia across different regions in AD. Future research should focus on validating these findings in larger and more diverse cohorts to enhance their translational potential.

Limitation and future prospect

This is the first attempt, and although the amount of spatial transcriptomics data is limited, we were still able to observe systematic and significant results with the available samples. The reliance on a limited number of spatial transcriptomics (AD ($N = 4$) and Control ($N = 3$) samples) may restrict the generalizability of our findings. Similarly, our analysis was confined to the Middle Temporal Gyrus and Frontal cortex, which may not capture the full spectrum of microglial diversity across different brain regions. To overcome these limitations and gain a more comprehensive understanding, future spatial studies encompassing additional vulnerable brain regions, such as the hippocampus, entorhinal cortex, and nucleus basalis, will be beneficial for mapping regional and disease-specific microglial responses. Also, future iterations of the reference atlas would benefit from additional iPSC-microglia models, particularly those involving xenotransplantation or organoid incorporation [54, 55]. As spatial transcriptomic technologies mature and larger, more anatomically diverse datasets become available, we anticipate that such analyses will provide deeper and more nuanced insights into the spatial dynamics of microglial populations with respect to amyloid plaque proximity and response [24, 56–58]. Our spatial analyses are inherently limited by their cross-sectional design, which prevents determination of prior microglial exposure to amyloid-β plaques and precludes distinguishing whether regional differences in microglial states reflect reduced pathological burden or enhanced clearance capacity. Additionally, a single amyloid-β marker limits characterization of plaque heterogeneity, which may influence microglial transcriptional responses [59].

Further, the Visium SD spatial transcriptomics platform is limited by its resolution, as each capture spot (< 55 μm) often contains transcripts from multiple cells,

which is improved from first report (capture > 10,000 transcripts per spot) [60]. This prevents accurate assignment of gene expression to individual microglia or other single-cell types. Consequently, our spatial analyses reflect spatially enriched transcriptomic signatures in areas likely containing microglia, rather than single-cell-level gene expression. To increase specificity, we focused on expression of well-established microglial markers and aligned these data with reference single-cell datasets to aid interpretation. Nonetheless, we acknowledge that cellular heterogeneity within each spot limits the resolution at which microglial states can be defined using this approach. Additionally, Human multiple-region (ROSMAP) study did not identify prominent microglia expression [16] corresponding to DAM, whereas our integrative approach was able to capture these particular profiles, but still those are not significantly associated with AD. These highlight that additional differences, including cohort's ascertainment, participants disease status, brain regions, neuropathological examination, and tissue handling play an important role and should be fully considered when interpreting this rich data.

Supplementary Information

The online version contains supplementary material available at https://doi.org/10.1186/s13195-025-01944-y.

Additional file 1: Selection of transcriptional states from each cohort

Additional file 2. Experimentally verified standard marker list collected from Yun Chen et al. (2021) [28] and Sun Victor et al (2023) [16].

Additional file 3. Differentially expressed genes between integrated clusters

Additional file 4. Enriched pathways for the upregulated genes within each integrated cluster

Additional file 5. Pairwise Pearson correlations between the log fold-changes of all differentially expressed genes from each cohort microglia subtype and our integrated microglial clusters

Additional file 6. Enriched pathways in upregulated genes between transcriptional states. Genes were identified using a linear mixed model comparing one state versus others

Additional file 7. Differential proportions of integrated clusters by phenotype. These tables display clusters enriched within certain phenotypes, determined using linear models (details provided at the bottom of each tab)

Additional file 8. Enriched pathways in upregulated genes between transcriptional states. Genes were identified using a linear mixed model comparing one state versus others

Additional file 9. Predicted cell scores using Seurat V5 label transfer of 56,454 iMGLs

Additional file 10. Fraction of predicted transcriptional states within each cortical layer

Additional file 11. Quantification of transcriptional states around proximal and distal Aβ/AT8 spots for Combined II-VI, External II-III, and Internal IV-VI cortical layers. Additionally, quantification of transcriptional states around proximal and distal Aβ/AT8 spots specifically in the External II-III layer across AD and CT samples

Additional file 12. IF stained P2RY12+ count, % area with P2RY12+ signal, Aβ+/-, and AT8+/- spots distribution in cortical layers II-III and IV-VI across all AD samples

Additional file 13. Document containing Supplementary figures S1-S9

Acknowledgements

We thank Dr. Gordon Meares and Dr. Subhodip Adhicary for their assistance with immunofluorescence microscopy imaging. This work was supported by access to equipment made possible by the Departments of Neurology and Psychiatry at Washington University School of Medicine and the Department of Neurology at The Ohio State University. This manuscript has been reviewed by Dian Study investigators for scientific content and consistency of data interpretation with previous DIAN Study publications. We acknowledge the altruism of the participants and their families and the contributions of the DIAN research and support staff at each participating site for contributions to this study. The results published here are in whole or in part based on data obtained from the AD Knowledge Portal (https://adknowledgeportal.org). Study data were provided by the Rush Alzheimer's Disease Center, Rush University Medical Center, Chicago. Data collection was supported through funding by NIA grants P30AG10161 (ROS), R01AG15819 (ROSMAP;genomics and RNAseq), R01AG17917 (MAP), R01AG30146, RF1AG57473 (single nucleus RNAseq), U01AG061356, R01AG066831, U01AG046152 as part of the AMP-AD consortium, and U01AG072572, the Illinois Department of Public Health (ROSMAP), and the Translational Genomics Research Institute (Genomic). Additional Phenotypic data can be requested at https://www.radc.rush.edu/.

Code availability

Custom code used to analyze the snRNA-seq and spatial transcriptomics datasets are available at https://github.com/HarariLab/Integration_work.git.

Authors' contributions

A.G. performed the quality control, bioinformatic analyses, interpreted the results, created the figures, and wrote the manuscript. A.C.B., S.V. and H.F. performed the P2RY12 immunostaining and quantification and review of the manuscript. A.C.B and S.A. performed CD68 immunostaining and quantification, drafted and review of the manuscript. I. D. S performed CD68 quantification, lead spatial transcript analyses of the FC, drafted and review of the manuscript, E.A., L.B., R.A. and A.N. interpreted the results. O.H. was involved in experiment design, analysis, data interpretation, intellectual contribution, and manuscript writing and review.

Funding

This work was possible thanks to the following governmental grants from the National Institute of Health: NIA R01AG057777 (OH), R56AG067764 (OH), U01AG072464 (OH), R01AG074012893 (OH), and R01AG075092 (H.F.). O.H. is an Archer Foundation Research Scientist. The funders of the study had no role in the collection, analysis, or interpretation of data, in the writing of the report, or in the decision to submit the paper for publication. Figure 1(a) was created with BioRender.com.

Data availability

The single nucleus data from the Knight ADRC accessed in this study are found in the National Institute on Aging Genetics of Alzheimer's Disease Data Storage Site (NIAGADS) with accession number NG00108 [https://www.niagads.org/datasets/ng00108]. The raw single nucleus data from the DIAN brain bank accessed in this study are available under restricted access to maintain individual and family confidentiality. These samples contain rare disease-causing variants that could be used to identify the participating individuals and families. Access can be obtained by request through the online resource request system on the DIAN Website: https://dian.wustl.edu/for-investigators/dian-observational-study-investigator-resources/.
The ROSMAP single nucleus RNA sequencing data used in this study are available at Synapse under Synapse ID syn52293417 [https://www.synapse.org/#!Synapse:syn52293417]. The xenografted microglia single cell RNA sequencing data used in this study was access from Christel Claes et al. (2021) [14]. CRISPR-based genetic screens in human iPSC-derived microglia used in this study available on NCBI GEO, accession number GSE178317. Dolan et al. (2023) [44] stem-cell-differentiated microglia (iMGLs) Seurat object was collected form authors upon request. SRT data from frontal cortex is available from NCBI GEO, accession number GSE263034 (sample GSM8184313). Source data is provided with this paper.

Declarations

Ethics approval and consent to participate
Not applicable.

Competing interests
The authors declare no competing interests.

Author details
[1]Department of Psychiatry, Washington University, Saint Louis, St. Louis, MO, USA
[2]The Charles F. and Joanne Knight Alzheimer Disease Research Center, Washington University, St. Louis, MO, USA
[3]Department of Neuroscience, OSU Wexner Medical Center, The Ohio State University, Columbus, OH, USA
[4]Department of Neurology, Division of Neurogenetics, The Ohio State University Wexner Medical Center, Columbus, OH, USA
[5]Chronic Brain Injury Program, The Ohio State University, Columbus, OH 43210, USA

Received: 11 June 2025 / Accepted: 16 December 2025
Published online: 28 December 2025

References

1. Esin RG, Safina DR, Khakimova AR, Esin OR. Neuroinflammation and neuropathology. Neurosci Behav Physiol. 2022;52:196–201. https://doi.org/10.1007/s11055-022-01223-5.
2. Miao J, Ma H, Yang Y, Liao Y, Lin C, Zheng J, et al. Microglia in Alzheimer's disease: pathogenesis, mechanisms, and therapeutic potentials. Front Aging Neurosci. 2023;15:1201982. https://doi.org/10.3389/fnagi.2023.1201982.
3. Wolf SA, Boddeke HWGM, Kettenmann H. Microglia in physiology and disease. Annu Rev Physiol. 2017;79(1):619–43. https://doi.org/10.1146/annurev-physiol-022516-034406.
4. Holtman IR, Skola D, Glass CK. Transcriptional control of microglia phenotypes in health and disease. J Clin Invest. 2017;127:3220–9. https://doi.org/10.1172/JCI90604.
5. Stratoulias V, Venero JL, Tremblay M, Joseph B. Microglial subtypes: diversity within the microglial community. EMBO J. 2019;38:e101997. https://doi.org/10.15252/embj.2019101997.
6. Garcia-Reitboeck P, Phillips A, Piers TM, Villegas-Llerena C, Butler M, Mallach A, et al. Human induced pluripotent stem cell-derived microglia-like cells harboring TREM2 missense mutations show specific deficits in phagocytosis. Cell Rep. 2018;24:2300–11. https://doi.org/10.1016/j.celrep.2018.07.094.
7. Hanger B, Couch A, Rajendran L, Srivastava DP, Vernon AC. Emerging developments in human induced pluripotent stem cell-derived microglia: implications for modelling psychiatric disorders with a neurodevelopmental origin. Front Psychiatry. 2020;11:789. https://doi.org/10.3389/fpsyt.2020.00789.
8. Mrza MA, He J, Wang Y. Integration of *iPSC*-derived microglia into brain organoids for neurological research. IJMS. 2024;25(6):3148. https://doi.org/10.3390/ijms25063148.
9. De Strooper B, Karran E. The cellular phase of Alzheimer's disease. Cell. 2016;164:603–15. https://doi.org/10.1016/j.cell.2015.12.056.
10. Long JM, Holtzman DM. Alzheimer disease: an update on pathobiology and treatment strategies. Cell. 2019;179:312–39. https://doi.org/10.1016/j.cell.2019.09.001.
11. Demirtaş M, Burt JB, Helmer M, Ji JL, Adkinson BD, Glasser MF, et al. Hierarchical Heterogeneity across Human Cortex Shapes Large-Scale Neural Dynamics. Neuron. 2019;101:1181-1194.e13. https://doi.org/10.1016/j.neuron.2019.01.017.
12. Brase L, You S-F, D'Oliveira Albanus R, Del-Aguila JL, Dai Y, Novotny BC, et al. Single-nucleus RNA-sequencing of autosomal dominant Alzheimer disease and risk variant carriers. Nat Commun. 2023;14:2314. https://doi.org/10.1038/s41467-023-37437-5.
13. Yu K, Hu Y, Wu F, Guo Q, Qian Z, Hu W, et al. Surveying brain tumor heterogeneity by single-cell RNA-sequencing of multi-sector biopsies. Natl Sci Rev. 2020;7:1306–18. https://doi.org/10.1093/nsr/nwaa099.
14. Claes C, Danhash EP, Hasselmann J, Chadarevian JP, Shabestari SK, England WE, et al. Plaque-associated human microglia accumulate lipid droplets in a chimeric model of Alzheimer's disease. Mol Neurodegener. 2021;16:50. https://doi.org/10.1186/s13024-021-00473-0.
15. Dräger NM, Sattler SM, Huang CTL, Teter OM, Leng K, Hashemi SH, et al. A CRISPRi/a platform in human iPSC-derived microglia uncovers regulators of disease states. Nat Neurosci. 2022;25:1149–62. https://doi.org/10.1038/s41593-022-01131-4.
16. Sun N, Victor MB, Park YP, Xiong X, Scannail AN, Leary N, et al. Human microglial state dynamics in Alzheimer's disease progression. Cell. 2023;186:4386-4403.e29. https://doi.org/10.1016/j.cell.2023.08.037.
17. Hao Y, Stuart T, Kowalski MH, Choudhary S, Hoffman P, Hartman A, et al. Dictionary learning for integrative, multimodal and scalable single-cell analysis. Nat Biotechnol. 2024;42(2):293–304. https://doi.org/10.1038/s41587-023-01767-y.
18. Hafemeister C, Satija R. Normalization and variance stabilization of single-cell RNA-seq data using regularized negative binomial regression. Genome Biol. 2019;20:296. https://doi.org/10.1186/s13059-019-1874-1.
19. Shannon CE. A mathematical theory of communication. Bell Syst Tech J. 1948;27:379–423. https://doi.org/10.1002/j.1538-7305.1948.tb01338.x.
20. Zimmerman KD, Espeland MA, Langefeld CD. A practical solution to pseudoreplication bias in single-cell studies. Nat Commun. 2021;12:738. https://doi.org/10.1038/s41467-021-21038-1.
21. He L, Davila-Velderrain J, Sumida TS, Hafler DA, Kellis M, Kulminski AM. NEBULA is a fast negative binomial mixed model for differential or co-expression analysis of large-scale multi-subject single-cell data. Commun Biol. 2021;4:629. https://doi.org/10.1038/s42003-021-02146-6.
22. Supek F, Bošnjak M, Škunca N, Šmuc T, Gibas C, editor. Revigo summarizes and visualizes long lists of gene ontology terms. PLoS ONE. 2011;6:e21800. https://doi.org/10.1371/journal.pone.0021800.
23. Chen S, Chang Y, Li L, Acosta D, Li Y, Guo Q, et al. Spatially resolved transcriptomics reveals genes associated with the vulnerability of middle temporal gyrus in Alzheimer's disease. Acta Neuropathol Commun. 2022;10:188. https://doi.org/10.1186/s40478-022-01494-6.
24. van Olst L, Simonton B, Edwards AJ, Forsyth AV, Boles J, Jamshidi P, et al. Microglial mechanisms drive amyloid-β clearance in immunized patients with Alzheimer's disease. Nat Med. 2025;31:1604–16. https://doi.org/10.1038/s41591-025-03574-1.
25. Kleshchevnikov V, Shmatko A, Dann E, Aivazidis A, King HW, Li T, et al. Cell 2location maps fine-grained cell types in spatial transcriptomics. Nat Biotechnol. 2022;40:661–71. https://doi.org/10.1038/s41587-021-01139-4.
26. Gabitto MI, Travaglini KJ, Rachleff VM, Kaplan ES, Long B, Ariza J, et al. Integrated multimodal cell atlas of Alzheimer's disease. Nat Neurosci. 2024;27:2366–83. https://doi.org/10.1038/s41593-024-01774-5.
27. Bankhead P, Loughrey MB, Fernández JA, Dombrowski Y, McArt DG, Dunne PD, et al. QuPath: open source software for digital pathology image analysis. Sci Rep. 2017;7:16878. https://doi.org/10.1038/s41598-017-17204-5.
28. Chen Y, Colonna M. Microglia in Alzheimer's disease at single-cell level. Are there common patterns in humans and mice? J Exp Med. 2021;218:e20202717. https://doi.org/10.1084/jem.20202717.
29. Paolicelli RC, Sierra A, Stevens B, Tremblay M-E, Aguzzi A, Ajami B, et al. Microglia states and nomenclature: a field at its crossroads. Neuron. 2022;110:3458–83. https://doi.org/10.1016/j.neuron.2022.10.020.
30. Astillero-Lopez V, Villar-Conde S, Gonzalez-Rodriguez M, Flores-Cuadrado A, Ubeda-Banon I, Saiz-Sanchez D, et al. Proteomic analysis identifies HSP90AA1, PTK2B, and ANXA2 in the human entorhinal cortex in Alzheimer's disease: potential role in synaptic homeostasis and Aβ pathology through microglial and astroglial cells. Brain Pathol. 2024. https://doi.org/10.1111/bpa.13235.
31. Krasemann S, Madore C, Cialic R, Baufeld C, Calcagno N, El Fatimy R, et al. The TREM2-APOE pathway drives the transcriptional phenotype of dysfunctional microglia in neurodegenerative diseases. Immunity. 2017;47:566-581.e9. https://doi.org/10.1016/j.immuni.2017.08.008.
32. Friedman BA, Srinivasan K, Ayalon G, Meilandt WJ, Lin H, Huntley MA, et al. Diverse brain myeloid expression profiles reveal distinct microglial activation states and aspects of Alzheimer's disease not evident in mouse models. Cell Rep. 2018;22:832–47. https://doi.org/10.1016/j.celrep.2017.12.066.
33. Marsh SE, Walker AJ, Kamath T, Dissing-Olesen L, Hammond TR, De Soysa TY, et al. Dissection of artifactual and confounding glial signatures by single-cell sequencing of mouse and human brain. Nat Neurosci. 2022;25:306–16. https://doi.org/10.1038/s41593-022-01022-8.
34. Wang S, Sudan R, Peng V, Zhou Y, Du S, Yuede CM, et al. TREM2 drives microglia response to amyloid-β via SYK-dependent and -independent pathways. Cell. 2022;185:4153-4169.e19. https://doi.org/10.1016/j.cell.2022.09.033.

35. Spangenberg E, Severson PL, Hohsfield LA, Crapser J, Zhang J, Burton EA, et al. Sustained microglial depletion with CSF1R inhibitor impairs parenchymal plaque development in an Alzheimer's disease model. Nat Commun. 2019;10:3758. https://doi.org/10.1038/s41467-019-11674-z.
36. Wes PD, Sayed FA, Bard F, Gan L. Targeting microglia for the treatment of Alzheimer's disease. Glia. 2016;64:1710–32. https://doi.org/10.1002/glia.22988.
37. Sun J, Nan G. The extracellular signal-regulated kinase 1/2 pathway in neurological diseases: a potential therapeutic target (Review). Int J Mol Med. 2017;39:1338–46. https://doi.org/10.3892/ijmm.2017.2962.
38. Porro C, Pennella A, Panaro MA, Trotta T. Functional role of non-muscle myosin II in microglia: an updated review. IJMS. 2021;22:6687. https://doi.org/10.3390/ijms22136687.
39. Gitik M, Reichert F, Rotshenker S. Cytoskeleton plays a dual role of activation and inhibition in myelin and zymosan phagocytosis by microglia. FASEB J. 2010;24:2211–21. https://doi.org/10.1096/fj.09-146118.
40. Liu C, Xu S, Liu Q, Chai H, Luo Y, Li S. Identification of immune cells infiltrating in hippocampus and key genes associated with Alzheimer's disease. BMC Med Genomics. 2023;16:53. https://doi.org/10.1186/s12920-023-01458-2.
41. Zenaro E, Pietronigro E, Bianca VD, Piacentino G, Marongiu L, Budui S, et al. Neutrophils promote Alzheimer's disease–like pathology and cognitive decline via LFA-1 integrin. Nat Med. 2015;21:880–6. https://doi.org/10.1038/nm.3913.
42. Fiala M, Liu QN, Sayre J, Pop V, Brahmandam V, Graves MC, et al. Cyclooxygenase-2-positive macrophages infiltrate the Alzheimer's disease brain and damage the blood–brain barrier. Eur J Clin Invest. 2002;32:360–71. https://doi.org/10.1046/j.1365-2362.2002.00994.x.
43. Hultman K, Strickland S, Norris EH. The APOE ε4/ε4 genotype potentiates vascular fibrin(ogen) deposition in amyloid-laden vessels in the brains of Alzheimer's disease patients. J Cereb Blood Flow Metab. 2013;33:1251–8. https://doi.org/10.1038/jcbfm.2013.76.
44. Dolan M-J, Therrien M, Jereb S, Kamath T, Gazestani V, Atkeson T, et al. Exposure of iPSC-derived human microglia to brain substrates enables the generation and manipulation of diverse transcriptional states *in vitro*. Nat Immunol. 2023;24:1382–90. https://doi.org/10.1038/s41590-023-01558-2.
45. Illes P, Rubini P, Ulrich H, Zhao Y, Tang Y. Regulation of microglial functions by purinergic mechanisms in the healthy and diseased CNS. Cells. 2020;9(5):1108. https://doi.org/10.3390/cells9051108.
46. Hashioka S, Inoue K, Otsuki K, Hayashida M, Wake R, Kawano N, et al. Contribution of "Genuine Microglia" to Alzheimer's Disease Pathology. Front Aging Neurosci. 2022;14:815307. https://doi.org/10.3389/fnagi.2022.815307.
47. Boche D, Gordon MN. Diversity of transcriptomic microglial phenotypes in aging and Alzheimer's disease. Alzheimers Dement. 2022;18:360–76. https://doi.org/10.1002/alz.12389.
48. Serneels L, Sierksma A, Pasciuto E, Geric I, Nair A, Martinez-Muriana A, et al. A versatile mouse model to advance human microglia transplantation research in neurodegenerative diseases. Mol Neurodegener. 2025;20:29. https://doi.org/10.1186/s13024-025-00823-2.
49. Kenkhuis B, Somarakis A, Kleindouwel LRT, van Roon-Mom WMC, Höllt T, van der Weerd L. Co-expression patterns of microglia markers Iba1, TMEM119 and P2RY12 in Alzheimer's disease. Neurobiol Dis. 2022;167:105684. https://doi.org/10.1016/j.nbd.2022.105684.
50. Sala Frigerio C, Wolfs L, Fattorelli N, Thrupp N, Voytyuk I, Schmidt I, et al. The major risk factors for Alzheimer's disease: age, sex, and genes modulate the microglia response to Aβ plaques. Cell Rep. 2019;27:1293-1306.e6. https://doi.org/10.1016/j.celrep.2019.03.099.
51. Mittal K, Eremenko E, Berner O, Elyahu Y, Strominger I, Apelblat D, et al. CD4 T cells induce a subset of MHCII-expressing microglia that attenuates Alzheimer pathology. iScience. 2019;16:298–311. https://doi.org/10.1016/j.isci.2019.05.039.
52. Tan Y-L, Yuan Y, Tian L. Microglial regional heterogeneity and its role in the brain. Mol Psychiatry. 2020;25:351–67. https://doi.org/10.1038/s41380-019-0609-8.
53. Masuda T, Sankowski R, Staszewski O, Böttcher C, Amann L, Sagar null, et al. Author Correction: Spatial and temporal heterogeneity of mouse and human microglia at single-cell resolution. Nature. 2019;568:E4. https://doi.org/10.1038/s41586-019-1045-2.
54. Mancuso R, Fattorelli N, Martinez-Muriana A, Davis E, Wolfs L, Van Den Daele J, et al. Xenografted human microglia display diverse transcriptomic states in response to Alzheimer's disease-related amyloid-β pathology. Nat Neurosci. 2024;27:886–900. https://doi.org/10.1038/s41593-024-01600-y.
55. Wong WJ, Zhu YW, Wang HT, Qian JW, Li Z, Li S, et al. Modeling hereditary diffuse leukoencephalopathy with axonal spheroids using microglia-sufficient brain organoids. Elife. 2025;13:RP96693. https://doi.org/10.7554/eLife.96693.
56. Wang P, Han L, Wang L, Tao Q, Guo Z, Luo T, et al. Molecular pathways and diagnosis in spatially resolved Alzheimer's hippocampal atlas. Neuron. 2025;113:2123-2140.e9. https://doi.org/10.1016/j.neuron.2025.03.002.
57. Ardura-Fabregat A, Bosch LFP, Wogram E, Mossad O, Sankowski R, Aktories P, et al. Response of spatially defined microglia states with distinct chromatin accessibility in a mouse model of Alzheimer's disease. Nat Neurosci. 2025;28:1688–703. https://doi.org/10.1038/s41593-025-02006-0.
58. Saito K, Goulding DS, Nolt GL, Dimas SH, Moore LC, Stevens IO, et al. High-Resolution Spatial Profiling of Microglia Reveals Proximity Associated Immunometabolic Reprogramming in Alzheimer's Disease. bioRxiv. 2025;2025.05.16.654329. https://doi.org/10.1101/2025.05.16.654329.
59. Sondag CM, Dhawan G, Combs CK. Beta amyloid oligomers and fibrils stimulate differential activation of primary microglia. J Neuroinflammation. 2009;6:1. https://doi.org/10.1186/1742-2094-6-1.
60. Ståhl PL, Salmén F, Vickovic S, Lundmark A, Navarro JF, Magnusson J, et al. Visualization and analysis of gene expression in tissue sections by spatial transcriptomics. Science. 2016;353:78–82. https://doi.org/10.1126/science.aaf2403.

Publisher's Note